EUROGRAPHICS - IEEE VGTC Symposium on Visualization (2005)
K. W. Brodlie, D. J. Duke, K. I. Joy (Editors)

Extending and Simplifying Transfer Function Design in Medical Volume Rendering Using Local Histograms

Claes Lundström†, Patric Ljung‡ and Anders Ynnerman‡

†Center for Medical Image science and Visualization (CMIV), Linköping University, and Sectra-Imtec AB
‡Norrköping Visualization and Interaction Studio (NVIS), Linköping University

Abstract

Direct Volume Rendering (DVR) is known to be of diagnostic value in the analysis of medical data sets. However, its deployment in everyday clinical use has so far been limited. Two major challenges are that the current methods for Transfer Function (TF) construction are too complex and that the tissue separation abilities of the TF need to be extended. In this paper we propose the use of histogram analysis in local neighborhoods to address both these conflicting problems. To reduce TF construction difficulty, we introduce Partial Range Histograms in an automatic tissue detection scheme, which in connection with Adaptive Trapezoids enable efficient TF design. To separate tissues with overlapping intensity ranges, we propose a fuzzy classification based on local histograms as a second TF dimension. This increases the power of the TF, while retaining intuitive presentation and interaction.

Categories and Subject Descriptors (according to ACM CCS): I.3.3 [Computer Graphics]: Picture/Image Generation; I.3.6 [Computer Graphics]: Methodology and Techniques; I.3.7 [Computer Graphics]: Three-Dimensional Graphics and Realism;

1. Introduction

Direct Volume Rendering (DVR) has been used in medical visualization research for many years and it is well known that DVR can be of significant diagnostic value when analyzing medical image volumes. The need for and benefit of DVR methods are underlined by the fact that traditional slice-by-slice viewing is becoming increasingly difficult [And03] for the large data sets produced in the current generation of imaging modalities. Furthermore, it has been shown that many types of clinical work benefit greatly from DVR, utilizing the exploratory possibilities of flexible Transfer Functions (TFs) and interactive data navigation.

In spite of its great potential DVR has not yet reached widespread use in non-research medical imaging. This paper addresses two, in our view, major obstacles for deployment of DVR in everyday clinical practice. In both cases, we make use of local histograms, i.e. properties that can be expressed in terms of histogram contents for local neighborhoods.

The first problem of DVR usage in the medical context is the high complexity of TF design. The currently available tools for TF construction and editing seldom remove the need for time-consuming manual adjustment. There is thus an urgent need to bring a substantial amount of automation into the design of TFs. This problem is particularly pertinent when dealing with MRI (Magnetic Resonance Imaging) data.

The traditional guiding tool used to find tissues of interest on the intensity scale is the global histogram. However, these tissues are often minor features, making their contribution invisible in the global histogram. We propose an automatic exhaustive detection of tissues, introducing *Partial Range Histograms* (PRHs) as a key concept. A PRH is populated by local neighborhoods in the data set that give a large footprint in a partial intensity range. Thereby the PRH can effectively expose obscured minor peaks. In combination, we introduce *Adaptive Trapezoids* that enable simple TF generation from the detected peaks represented by the PRHs.

† clalu@imv.liu.se
‡ {plg,andyn}@itn.liu.se

The second problem of focus in this paper is a limitation of 1D TFs, namely the failure to separate tissues with overlapping intensity ranges. We approach this problem by deriving neighborhood characteristics to make a fuzzy classification of the voxels in the overlapping range. The classification value is used as a second attribute for the voxels, which in connection with a 2D TF results in an enhanced rendering. The second TF dimension is constructed as a linear interpolation of the tissue-specific trapezoids, avoiding added complexity for the user.

Our TF framework is based on traditional color-opacity trapezoids. This model fits a work flow that we believe is very intuitive: to identify materials in an intensity scale and then assign visual features to them. Our focus is on medical DVR, but we believe that the methods are applicable to other DVR domains as well. The major contributions are the following:

- Automatic exhaustive peak detection based on Partial Range Histograms
- Simplified TF construction using Adaptive Trapezoids
- Extended TF capabilities using classification probability as a second TF dimension

2. Related work

The difficulty of TF construction is a problem that has been acknowledged in previous research. Bajaj et al. [BPS97] introduced the Contour Spectrum, which analyzes isosurface properties for the whole intensity value range. The primary use is to guide a choice of appropriate values for isosurfacing. A different TF design technique is to automatically render many thumbnails with various TF settings and let the user explore that "gallery" [HHKP96, MAB*97]. There is a similar approach in the medical context [KG01], where the user interface has several levels of complexity for the user to choose from. Another way to avoid traditional TF construction is data probing, where multiple voxel attributes can be automatically integrated in the rendering [TLM03].

TF construction is closely related to classification challenges. Segmentation methods in medical imaging often employ specialized models based on domain knowledge for the task at hand. One recent example is a method to segment hip joints [ZSS*03]. It is difficult to extend these methods into general-purpose tools, since time-consuming user interaction would be required in many situations. A commonly addressed problem of MRI data sets is the Partial Volume effect, i.e. that a voxel can contain multiple tissues. Small neighborhoods have been used to reconstruct the tissue composition within each voxel [LFB98]. This subvoxel classification task is not addressed in this paper.

Two-dimensional TFs were introduced in 1988 by Levoy [Lev88], suggesting gradient magnitude as a second dimension. Kindlmann and Durkin [KD98] proposed a TF model

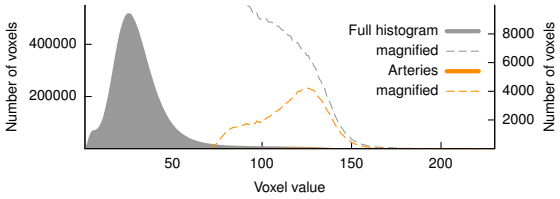

Figure 1: *Histogram of MR renal arteries data set, full and magnified scale. The main peak completely dominates the minor peak from the arteries (orange), which is the interesting tissue. In full scale, the artery peak is hardly visible.*

by adding the first and second derivative along the gradient direction as extra attributes for a voxel. This 3D histogram yields good separation of material boundaries and enables a more advanced rendering. This model has been extended with TF design tools [KKH02], among others a data probe with which a user can capture local characteristics. Curvature-based TFs classify surfaces according to their shape and have been shown to add visualization possibilities [HKG00], [KWTM03], e.g. separation within an isosurface.

Recent work by Lum and Ma [LM04] also explores visualization of material boundaries. During rendering, an additional gradient aligned sample is retrieved, capturing boundary properties. With two scalars for each sample, a 2D lighting TF can be applied. As a preliminary result, this additional attribute is used for one case of material classification.

It is worth noting that the above multidimensional TFs are primarily intended to display material boundaries. This type of rendering is not sufficient for the tasks of medical visualization. One reason is inherent noise that distorts the boundaries [PBSK00], another is that the density of a tissue is often important for the diagnostic work. There are methods that go further than pure boundary analysis, by deriving local structure properties as a base for classification [SWB*00]. However, separation of unstructured tissues of similar intensity is not addressed by neither structure nor gradient approaches.

3. Automatic exhaustive tissue detection

In MRI, volume rendering is a very rare tool. MRI data sets have the great drawback compared to CT data sets that there is no calibrated intensity scale. The global histogram is then the main guide when designing TFs. The task of identifying tissues in the histogram would be easy if they corresponded to visible peaks. However, this is seldom the case, an example is seen in figure 1. The single dominant peak consists of unimportant features. We propose an unsupervised detection scheme based on the PRH concept, aiming at finding all tissues in the histogram.

3.1. Partial Range Histograms

A PRH is the histogram for a set of neighborhoods that are typical for a given intensity range. The neighborhoods can have arbitrary shape, but must fill the volume and be non-overlapping. We use PRHs based on cubic block neighborhoods. To select the blocks to be part of a PRH, we define the *range weight* w_r, see equation 1, measuring the size of the neighborhood footprint in the partial range.

$$w_r(\Phi, N) = \frac{|N \cap V_\Phi|}{|N|} \tag{1}$$

N is an arbitrary voxel neighborhood, V_Φ is the set of voxels within a range Φ. $|V|$ denotes the number of voxels in a set V. A block is added to the PRH if the range weight is high enough: $w_r \geq \varepsilon$. The data set characteristics determine the threshold, we use $\varepsilon = 0.95$ to capture narrow features and $\varepsilon = 0.5$ to pick up inhomogeneous regions. A block size of 8^3 is used in this paper. This choice is a trade-off between the simplicity of large blocks and the sensitivity for narrow features of small blocks. Note that a PRH does not need to find all blocks containing a material, since the *position* of the PRH is the main input to TF construction, not the height.

3.2. Exhaustive multiple-peak search

We propose a fully automatic analysis of the global histogram that employs iterative subdivision of the histogram, with the goal of detecting all peaks corresponding to distinct materials. The core component of our approach is the PRH defined above. The steps of the algorithm are:

1. Find the highest peak of the main histogram.
2. Fit a Gaussian to the peak.
3. Create a PRH for the middle part of the Gaussian.
4. Remove the PRH blocks from the main histogram.
5. Run steps 1-4 until the main histogram is empty.
6. Merge peaks that are similar.

The algorithm starts with the full histogram range. The highest peak is identified and a Gaussian curve is fitted to its shape. The Gaussian is described by its midpoint μ, height $\hat{h}$, and deviation σ. The fitting process minimizes the accumulated height difference between the histogram and the middle part of the Gaussian. The error summation range is $\mu \pm \alpha\sigma$, where $\alpha = 1$ in this case. This small range is chosen since it often occurs that only the tip of the histogram peak is visible.

The next step is to create a PRH for the range $\mu \pm \sigma$. This range choice yields many narrow, accurate peaks. Since the merging step follows, an abundance of peaks is not a problem here. The PRH is stored and then removed from the main histogram. This exposes a new peak and the algorithm restarts. If a PRH is empty, the ε value is lowered and step 3 is performed again. All blocks are thus guaranteed to become part of a PRH. Then a merging of similar peaks takes place. To describe the peaks, we fit a Gaussian to each PRH with the same method as above. Here $\alpha = 2$, since the whole peak is exposed. Peaks are joined if they have similar deviation, $\sigma_{max}/\sigma_{min} \leq 4$, while their means are close, $\mu_{max} - \mu_{min} \leq \sigma_{min} \cdot \max(1.0, 2.0 - \sigma_{min}/40.0)$. The second criterion is thus less strict for narrow peaks. For merged peaks, a new Gaussian is fitted to allow multiple mergers. We will use the term PRH also for these merged PRHs.

3.3. Adaptive Trapezoids

The use of PRHs can be taken one step further, to semi-automatically generate TFs. To this end we suggest the *Adaptive Trapezoid*. This trapezoid is a TF component that adapts center, width, and shape to the Gaussian approximation of the current PRH, see figure 2. Adaptive Trapezoids enable a highly efficient work flow when manually defining a TF from scratch, as follows:

1. Apply automatic tissue detection.
2. Activate an Adaptive Trapezoid. At this stage, the TF consists of this single trapezoid.
3. Browse the detected PRHs until the adapted trapezoid highlights an interesting tissue.
4. Fixate the trapezoid at this position, making it static and temporarily disconnected from the TF.
5. Perform steps 2-4 until all tissues are found.
6. View the full TF, i.e. activate all defined trapezoids. Adjust the color and opacity of each trapezoid.

In addition, Adaptive Trapezoids can be used as a manual tissue exploration tool for the user. Step 1 above is then removed and step 3 is replaced by manually sliding the center of a partial range across the intensity scale.

4. Separating overlapping tissue ranges

A common problem in medical DVR is tissues with overlapping intensity ranges. A typical example is CT angiographies, where vessels with contrast agent has the same intensity as spongy bone. A TF based on intensity only cannot achieve a rendering that well separates the two tissues, see figure 7. We will show that local histogram analysis can extend the capabilities in this respect. Such an application of neighborhood operators to classify voxels can be seen as a type of morphological filtering [MS90].

4.1. Classification probability

When the intensity alone cannot separate materials, neighborhood histogram analysis is often a sufficient tool. The basic idea is that the different surroundings of equal-intensity voxels can provide diversifying information. In this paper, the analysis is based purely on range weights, see section 3.1, but other information derived from local histograms could also be used.

We will now describe our method using the example of

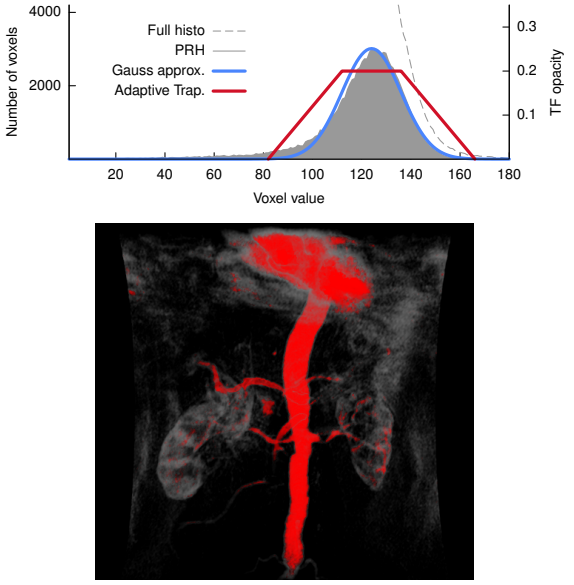

Figure 2: *Adaptive Trapezoid. Top: The peak detection results in a PRH (gray), to which a Gaussian is fitted (blue), which defines the Adaptive Trapezoid (red). Bottom: The resulting rendering. A low-opacity gray ramp is added to the TF for clarity.*

the heart data set in figure 8. The classification goal is to separate the coronary artery from the large vessels. To this end, domain knowledge of the physician is used. A first criterion is: "The coronary artery is more narrow than other vessels". We define Φ_1 as the mutual range of all vessels. The narrowness can then be described as the range weight $w_r(\Phi_1)$. The next step is to let the physician define the range weights where the classification is confident. For instance, for a range weight of 0.3 a voxel can confidently be assumed to be part of a large vessel, whereas 0.1 confidently implies a coronary artery voxel. These confidence levels are denoted w_{A1} and w_{B1}, respectively.

The next step is to create a measure p_1, being the classification certainty from the narrowness criterion. We choose a signed representation, where the sign denotes the most likely tissue (here: negative for large vessels) and the magnitude is the confidence of the classification. This form is achieved as described in equations 2 and 3, where $\mathbf{C_2}$ is a function that clamps to the $[-2.0, 2.0]$ interval. The resulting function is shown in figure 3.

$$\mu_1 = (w_{A1} + w_{B1})/2, \quad \delta_1 = (w_{B1} - w_{A1})/2 \tag{2}$$

$$p_1 = \mathbf{C_2}\Big((w_r(\Phi_1) - \mu_1)/\delta_1\Big) \tag{3}$$

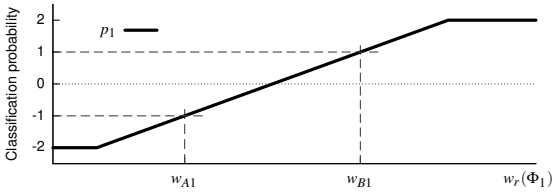

Figure 3: *Classification probability. The probability p_1 is a function of the range weight $w_r(\Phi_1)$. The transformation is defined by the confidence levels w_{A1} and w_{B1}.*

A second criterion from domain knowledge is: "The coronary artery is close to the heart muscle". We define Φ_2 as the range of muscle tissue. This proximity criterion can then be described as $w_r(\Phi_2)$. As for the narrowness, the physician defines two confidence levels w_{A2} and w_{B2} corresponding to confident classification as either material. The classification certainty p_2 is derived in the same way as p_1, see equation 3. The total classification certainty $\mathbf{P}$ is defined as a weighted sum of p_1 and p_2.

The general definition of $\mathbf{P}$, valid for the separation of any two materials A and B, is given in equation 4. There are n materials used for diversifying criteria, defined by the ranges Φ_1 through Φ_n. Each p_i is derived in accordance with equation 3. It is possible to steer the contribution from each criterion with the weights λ_i, but equal weighting is used throughout this paper. $\mathbf{P}$ is clamped to the $[-1.0, 1.0]$ interval, where the extreme values correspond to fully certain classification. Since the p_i components have a wider range, $[-2.0, 2.0]$, "extra" confidence from one component can dominate an uncertain classification in another.

$$\mathbf{P} = \mathbf{C_1}\Big(\sum_{i=1}^{n} \lambda_i p_i\Big), \quad \text{where} \sum_{i=1}^{n} \lambda_i = 1 \tag{4}$$

In summary, the algorithm requires an a priori analysis of how neighborhood materials can achieve the wanted separation of A and B. The information needed for each material is the range Φ along with the reference levels w_A and w_B. Note that w_A and w_B can have "unnatural" values outside $[0.0, 1.0]$. For instance, if a range weight ≥ 0.5 confidently implies tissue B, whereas 0.0 corresponds to equal probability of either tissue, then $w_B = 0.5$ and $w_A = -0.5$.

4.2. TF construction

To separate the tissues in the rendering, our approach is to use the classification probability $\mathbf{P}$ from above as a second attribute for each voxel in an overlapping range. This yields a multivariate data set, where the second value is solely intended to separate the overlapping tissues. In the general case we have an arbitrary number of tissues, whose ranges

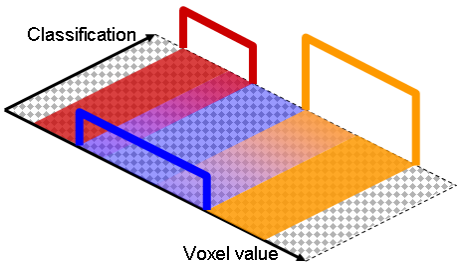

Figure 4: *2D TF. The traditional 1D TF is extended with a material classification dimension. Trapezoids for overlapping materials are placed at extreme classification values and the 2D TF is interpolated in between them.*

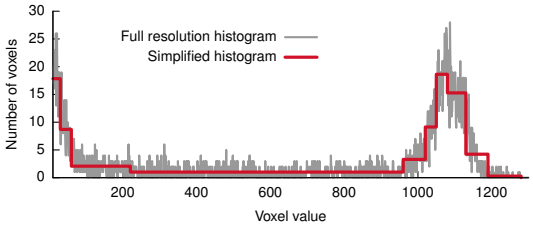

Figure 5: *A block histogram from a medical CT volume and its piece-wise constant approximation using 12 segments.*

may partly overlap. We restrict the discussion to no more than two overlapping tissues at any intensity value. This restriction is not very limiting in the medical domain.

To render this multivariate data set, we propose a novel type of 2D TF that is completely defined by tissue-centric trapezoids. Each trapezoid is placed at either extreme of the classification dimension in a way that overlapping trapezoids are always on opposite sides, see figure 4. The second dimension is filled by linear interpolation of the 1D TFs at the extremes. The interpolation is only necessary for overlapping intensity ranges, for other ranges the 1D trapezoid at one of the extremes is used.

This approach has a number of desirable features. It is natural for the user to design a TF where one tissue at a time looks good. The Adaptive Trapezoid work flow from section 3.3 is well suited to this task. The automatic interpolation of the second dimension then enables the power of a 2D TF without introducing complexity to the user. Another appealing property is that the classification dimension integrates a fuzzy segmentation into the rendering, reducing the impact of misclassification artifacts.

The implementation used in this paper is further simplified. The used data sets have 12 bit precision, leaving 4 bits unused. The value of **P**, which does not need to be very precise, is entered in these top 4 bits.

4.3. Neighborhood types

Three different types of voxel surroundings are used in this paper: single block, voxel-centric, and double block neighborhoods. *Single block neighborhoods* are obtained by a static subdivision of non-overlapping blocks, typically cubes. This is an efficient but coarse representation of neighborhood properties that was used for PRHs above. A *voxel-centric neighborhood* is more precise, since the region varies for each position in the volume. For further accuracy, we define that the voxel itself is not part of the neighborhood. In our voxel-centric examples we use a spherical neighborhood of radius 7, since this choice has proven to yield reliable statistics for many anatomical features.

Unfortunately, large voxel-centric neighborhoods require extensive computation. As a complement, we therefore propose a *double block neighborhood* that yields voxel-specific statistics while being fast to process. Two separate block subdivisions are applied to the volume, where one is shifted half a block size in all dimensions. Thus, each voxel is a member of exactly two blocks. Any neighborhood measure for a voxel is then simply derived as a linear combination of the values calculated for the two blocks it belongs to. The interpolation weights c_1 and c_2 are determined through two criteria: they are inversely proportional to the distance to the center of each block (d_1 and d_2) and the sum is 1 for each voxel, see equation 5. The block size in this paper is 8^3 voxels also for double block neighborhoods.

$$\begin{cases} c_1 + c_2 = 1 \\ c_1/c_2 = d_2/d_1 \end{cases} \Leftrightarrow \begin{cases} c_1 = d_2/(d_1+d_2) \\ c_2 = d_1/(d_1+d_2) \end{cases} \quad (5)$$

An additional simplification is to avoid the use of fully resolved block histograms. For double block neighborhoods, we employ the histogram simplification approach of our previous work [LLYM04]. The simplification is based on piece-wise constant segments, see figure 5. This method has proven to efficiently preserve the shape of the histogram, especially the peaks. For more details we refer to our previous paper. In this paper, the simplification consists of 12 segments with a minimum width of 10.

5. Results

5.1. Tissue detection

We have tested our schemes on a number of data sets from actual clinical use at CMIV. First we turn to the results of the automatic tissue detection. The correct peaks were defined by manual segmentation for each distinct tissue. Some peak detection results are presented in figure 6. Very large and very small peaks have been left out for clarity, our tests resulted in a total number of 5-10 peaks for each data set.

The first case is an MR examination of the biliary duct,

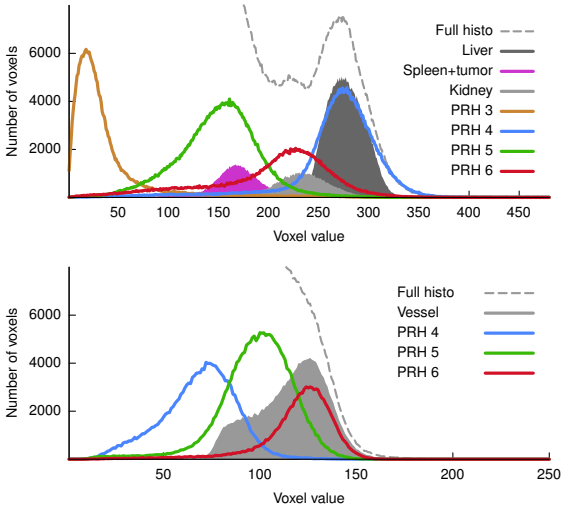

Figure 6: *Automatic peak detection. Top: MR biliary duct data set,* $\varepsilon = 0.5$*. The position of the segmented peaks correspond well to the automatic detection. Bottom: MR renal arteries data set,* $\varepsilon = 0.95$*. One of the detected peaks coincides well with the true peak from the segmentation.*

where the distinct tissues are liver, kidney, spleen and tumor. The spleen and the tumor are treated as one tissue below, since their histograms fully coincide. The automatic peak detection performs well in finding the position of the tissue peaks. The height estimation varies in accuracy, depending on the extent of other soft tissue in the same intensity range. Deviations in height are a minor concern, since they have little effect on subsequent TF construction. Not surprisingly, the biliary duct is not found. Its histogram shows diffuse spikes below height 20, hardly characterizable as a peak.

The second case of figure 6 is an MR angiography of the renal arteries (see also figure 2). The single interesting peak corresponds to the vessels with contrast agent. Despite the extreme difference in height compared to the main peak (4.2k vs 520k voxels), the detection scheme accurately locates the vessel peak: the true value being 126, μ is found at 124. The height is slightly underestimated, since the narrow vessels do not dominate all their neighborhoods.

5.2. Tissue separation

The 2D TF approach of section 4.2 has been tested on a CT pelvis angiography data set. The neighborhoods tested are of both voxel-centric spherical and double block type. The parameters of **P** were derived by manually probing the volume. Vessel voxels were characterized by neighborhoods with much soft tissue and little dense bone. The resulting renderings are shown in figure figure 7. The methods very well separate the two tissues. The diagnostic value is enhanced since the vessels are not disturbed by red bone in the background. Even the difficult task of preserving thin vessels close to bone is successful. The fuzzy segmentation shows uncertain regions in pink, letting the user make the ultimate classification decision. The spherical neighborhood achieves a smooth classification. The double block approach yields faint speckle artifacts in the bone, but performs well in spite of its simplicity.

The separation can also be applied to identical tissues. An example for a CT angiography of the heart is given in figure 8. The 1D TF makes all vessels and heart ventricles bright, since they are all filled with contrast agent. However, the primary objective of the examination is to study the coronary arteries. With **P** as a second attribute, it is possible to highlight only narrow vessels close to muscle tissue. Hence, the visually disturbing large bright regions are removed. A voxel-centric spherical surrounding provides high image quality. The double block neighborhood causes artifacts for large vessel boundaries, being mistaken for narrow vessels, whereas the coronary artery shows few artifacts.

A final example on tissue separation is the MR biliary duct volume of section 5.1, see figure 9. There is a large liver tumor that is seen as a slightly darker region when rendering the liver only. A 1D TF for the tumor is useless, since it becomes obscured by unimportant tissue. When introducing the classification dimension to emphasize homogeneous regions with few low-intensity neighbors, the tumor as well as the spleen (top right) are clearly rendered.

As expected, the performance for the large spherical neighborhood is low and heavily dependent on the number of voxels in the overlapping range. The classification requires about 0.02 ms per overlapping voxel, running a 1.8 GHz Intel Pentium M laptop. This amounts to 32 s for the pelvis angiography data set and 350 s for the heart. With the double block approach, these times are reduced to 0.65 s and 1.85 s, respectively, of which about 60% is spent adapting the classification value to the 4-bit format.

6. Conclusions

In this paper we proposed the use of local histogram analysis to simplify, but also to extend TF design. The simplification achieved by automatic tissue detection and Adaptive Trapezoids is one step further towards a streamlined work flow of medical volume rendering. Preliminary results show that having detected all tissue peaks with our scheme, it is feasible to automatically adapt TFs between data sets of similar examination types. Peaks that resemble each other, mainly in terms of $\hat{h}$ and σ, can be identified as the same tissue. A TF connected to the tissues can then easily be repositioned. A future research goal is to verify the achieved simplicity in user studies and to further simplify the work flow.

For the more advanced user, voxel neighborhood properties are shown to extend the TF capabilities. We believe

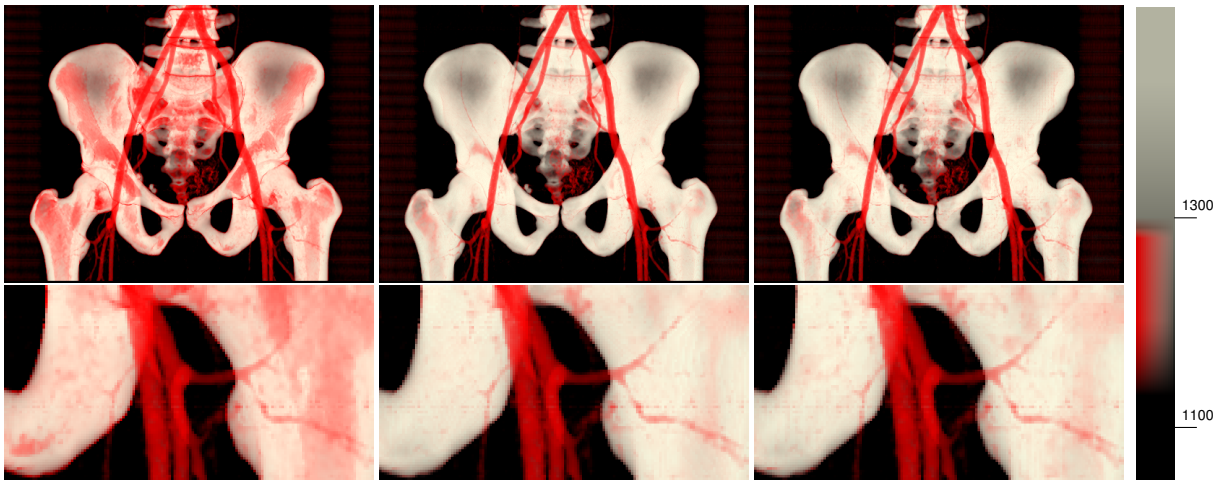

Figure 7: *Separation of spongy bone and vessels. Left: With a 1D TF, spongy bone turns red. Middle: With a classifying 2D TF, voxel-centric nbh, the vessels stand out from the background* (w_{A1}=0.0,w_{B1}=0.1,w_{A2}=0.2,w_{B2}=−0.1). *Right: A classifying 2D TF for double block nbh achieves the separation with minor artifacts* (w_{A1}=0.0,w_{B1}=0.05,w_{A2}=0.2,w_{B2}=−0.2). *Ranges:* Φ_1=[1300,2000],Φ_2=[900,1150].

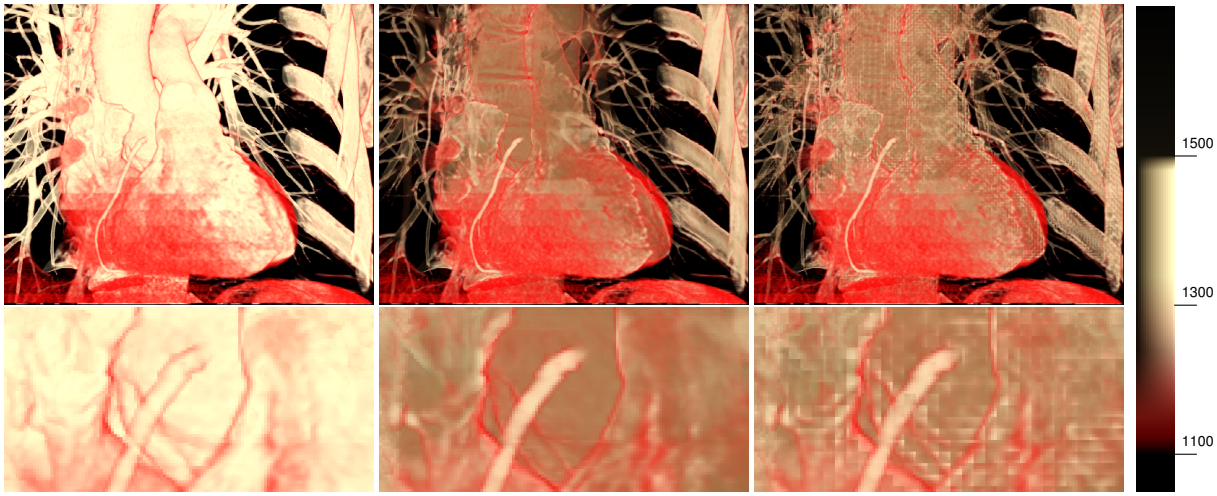

Figure 8: *Highlighting a coronary artery. Left: With a 1D TF, the brightness of the large vessels disturb the study of the coronary artery. Middle: With a classifying 2D TF, voxel-centric nbh, the coronary artery stands out* (w_{A1}=0.3,w_{B1}=0.1,w_{A2}=0.2,w_{B2}=0.4). *Right: A classifying 2D TF for double block nbh also highlights the coronary artery, while introducing speckle artifacts at the large vessel boundaries* (w_{A1}=0.5,w_{B1}=0.2,w_{A2}=0.2,w_{B2}=0.4). *Ranges:* Φ_1=[1300,1500],Φ_2=[900,1150].

that the framework of this paper can be used for many complex rendering tasks. So far, our tissue separation scheme requires some parameter tuning. Future work includes reducing this need, e.g. by employing the automatic peak detection to adapt these parameters between data sets, as in TF adaptation. We also aim to raise the performance/quality trade-off to a higher level.

Acknowledgements

This work has been conducted within the Center for Medical Image Science and Visualization (CMIV) at Linköping University, Sweden. CMIV is acknowledged for provision of financial support and access to leading edge research infrastructure. The authors would like to thank Anders Persson, MD, for many fruitful discussions. This work has been funded by the Swedish Research Council, grants 621-2003-6582 and 621-2001-2778, and the Swedish Foundation for

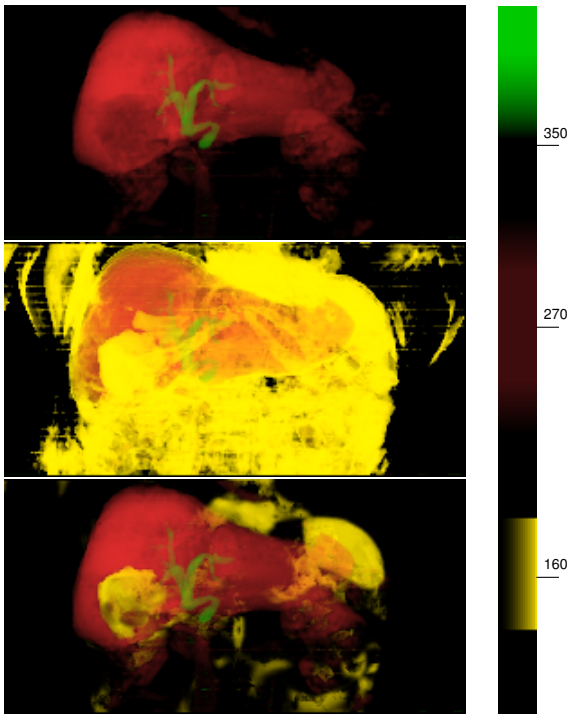

Figure 9: *Highlighting of liver tumor. Top: 1D TF rendering, the tumor area is slightly darker than the liver. Middle: An attempt to highlight the tumor with a 1D TF. Bottom: A classifying 2D TF, voxel-centric nbh, clearly highlights the tumor and the spleen* (w_{A1}=0.1,w_{B1}=0.6,w_{A2}=0.2,w_{B2}=0.1,Φ_1=[150,200],Φ_2=[0,140]).

Strategic Research, grant A3 02:116. The authors are pursuing patent applications based on this work.

References

[And03] ANDRIOLE K. P.: A position paper from the SCAR TRIP(tm) subcommittee. http://www.scarnet.org/pdf/-TRIPwhitepaper1103.pdf, November 2003. Acquired March 2004.

[BPS97] BAJAJ C., PASCUCCI V., SCHIKORE D. R.: The Contour Spectrum. In *Proceedings IEEE Visualization 1997* (1997), pp. 167–173.

[HHKP96] HE T., HONG L., KAUFMAN A., PFISTER H.: Generation of transfer functions with stochastic search techniques. In *Proceedings IEEE Visualization 1996* (1996), pp. 227–234.

[HKG00] HLADUVKA J., KÖNIG A. H., GRÖLLER E. M.: Curvature-based transfer functions for direct volume rendering. In *Proceedings Spring Conference Computer Graphics 2000* (2000), vol. 16, pp. 58–65.

[KD98] KINDLMANN G., DURKIN J. W.: Semi-automatic generation of transfer functions for direct volume rendering. In *Proceedings IEEE Symposium on Volume Visualization* (1998), pp. 79–86.

[KG01] KÖNIG A. H., GRÖLLER E. M.: Mastering transfer function specification by using VolumePro technology. In *Proceedings Spring Conference Computer Graphics 2001* (2001), vol. 17, pp. 279–286.

[KKH02] KNISS J., KINDLMANN G., HANSEN C.: Multidimensional transfer functions for interactive volume rendering. *IEEE Transactions on Visualization and Computer Graphics 8* (2002), 270–285.

[KWTM03] KINDLMANN G., WHITAKER R., TASDIZEN T., MÖLLER T.: Curvature-based transfer functions for direct volume rendering: Methods and applications. In *Proceedings IEEE Visualization 2003* (2003), pp. 513–520.

[Lev88] LEVOY M.: Display of surfaces from volume data. *IEEE Computer Graphics and Applications 8*, 5 (1988), 29–37.

[LFB98] LAIDLAW D., FLEISCHER K., BARR A.: Partial-volume bayesian classification of material mixtures in MR volume data using voxel histograms. *IEEE Transactions on Medical Imaging 17*, 1 (1998), 74–86.

[LLYM04] LJUNG P., LUNDSTRÖM C., YNNERMAN A., MUSETH K.: Transfer Function Based Adaptive Decompression for Volume Rendering of Large Medical Data Sets. In *Proceedings IEEE Volume Visualization and Graphics Symposium* (2004), pp. 25–32.

[LM04] LUM E. B., MA K.-L.: Lighting transfer functions using gradient aligned sampling. In *Proceedings IEEE Visualization 2004* (2004), pp. 289–296.

[MAB*97] MARKS J., ANDALMAN B., BEARDSLEY P., FREEMAN W., GIBSON S., HODGINS J., KANG T., MIRTICH B., PFISTER H., RUML W., RYALL K., SEIMS J., SHIEBER S.: Design galleries: A general approach to setting parameters for computer graphics and animation. In *Proceedings SIGGRAPH 1997* (1997), pp. 389–400.

[MS90] MARAGOS P., SHAFER R. W.: Morphological systems for multidimensional signal processing. *Proceedings of the IEEE 78*, 4 (1990), 690–710.

[PBSK00] PFISTER H., BAJAJ C., SCHROEDER W., KINDLMANN G.: The transfer function bake-off. In *Proceedings IEEE Visualization 2000* (2000), pp. 523–526.

[SWB*00] SATO Y., WESTIN C.-F., BHALERAO A., NAKAJIMA S., SHIRAGA N., TAMURA S., KIKINIS R.: Tissue classification based on 3D local intensity structures for volume rendering. *IEEE Transactions on Visualization and Computer Graphics 6*, 2 (2000), 160–179.

[TLM03] TZENG F.-Y., LUM E. B., MA K.-L.: A novel interface for higher-dimensional classification of volume data. In *Proceedings IEEE Visualization 2003* (2003), pp. 505–512.

[ZSS*03] ZOROOFI R. A., SATO Y., SASAMA T., SUGANO N., YONENOBU K., YOSHIKAWA H., OCHI T., TAMURA S.: Automated segmentation of acetabulum and femoral head from 3-D CT images. *IEEE Transactions on Information Technology in Biomedicine 7*, 4 (December 2003), 329–343.